

A Nonlinear Model of fMRI BOLD Signal Including the Trend Component

Takashi Matsubara, Hiroyuki Torikai, Tetsuya Shimokawa, Kenji Leibnitz, and Ferdinand Peper

Abstract—This paper presents a nonlinear model of the human brain activity response to visual stimuli according to *Blood-Oxygen-Level-Dependent (BOLD)* signals scanned by *functional Magnetic Resonance Imaging (fMRI)*. A BOLD signal usually contains a low frequency signal component (*trend*), which is often ignored by the existing models or removed by approximation methods. However, such detrending could also destroy the dynamics of the BOLD signal and miss an important response. This paper shows a model that, in the absence of detrending, can predict the BOLD signal with smaller errors than existing models. For detrending, the presented model has also a lower Schwarz information criterion than existing models, which implies that the presented model will be less likely to overfit the experimental data.

I. INTRODUCTION

Responses and interactions of human brain regions are being investigated as they contribute to the mapping of the brain network topology and the understanding of the brain functions. The responses of the brain regions are sampled by using *functional Magnetic Resonance Imaging (fMRI)*, which detects the *Blood-Oxygen-Level-Dependent (BOLD)* signals; the scanned spatial unit is called a *voxel*, which is several mm in size in all three dimensions. Traditionally, the responding voxels have been identified by using cross correlation [1] and covariance [2], [3] between the inputs stimuli and the BOLD signals. The BOLD signals are predicted by the *General Linear Model (GLM)* [4]–[9]; this is done under the assumption that they are the sum of the input stimuli without any dynamics considered. On the other hand, the brain voxel dynamics and their interactions represented by BOLD signals are often modeled in more complicated ways, like the *Multivariable Regressive Model (MRM)* [10]–[13] and the *Balloon Model (BM)* [14]–[17].

The BOLD signal contains a low frequency signal called *drift* or *trend* [6], [18]–[21], which is thought to be caused by scanner noise, physiological noise, or other physiological pulsations. The trend component is often removed (*detrended*) by using linear or higher order polynomials, spline approximation, wavelet transformation, or Fourier transformation. Unfortunately, detrending not only removes meaningless signals, but also distorts the dynamics of voxels.

Takashi Matsubara is with the Graduate School of Engineering Science, Osaka University, Osaka 560-8531, Japan, Hiroyuki Torikai is with Faculty of Computer Science and Engineering, Kyoto Sangyo University, Kyoto 603-8555, Japan, and Tetsuya Shimokawa, Kenji Leibnitz, and Ferdinand Peper are with Center for Information and Neural Networks (CiNet), National Institute of Information and Communications Technology, and Osaka University, 1-4 Yamadaoka, Suita, Osaka 565-0871, Japan. E-mails: matubara@hopf.sys.es.osaka-u.ac.jp, torikai@cse.kyoto-su.ac.jp, shimokawa@nict.go.jp, leibnitz@nict.go.jp, and peper@nict.go.jp.

This work was supported by Grant-in-Aid for JSPS Fellows

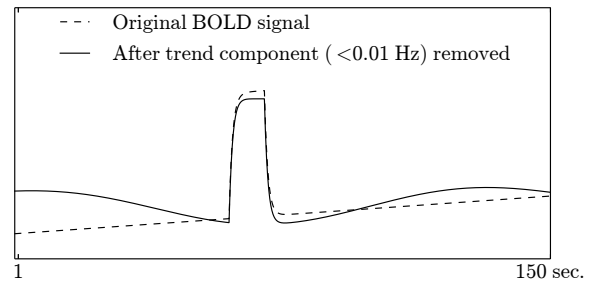


Fig. 1. Conceptual BOLD signal (the dashed line) and the detrended BOLD signal (the solid line). The original BOLD signal has no undershoots, but the detrended BOLD signal has something like undershoots before and after the response.

For example, an initial increase in oxygen consumption in response to a stimulus prior to the blood flow increase sometimes causes the undershoot prior to the BOLD signal to increase rapidly; this undershoot is called *initial dip* [15], [16]. This phenomenon is important, since the point of time at which the voxel responds to the stimulus is not the point of time marking the start of the BOLD signal's increase, but the time of the initial dip. However, even if the BOLD signal has no undershoot, detrending by Fourier transformation can fake it as shown in Fig. 1, and, thus, detrending could lead to a wrong estimation of the response time and relationships between voxels. Therefore, investigations of the dynamics and interactions of voxels require a model of the BOLD signal that does not rely on detrending.

This paper presents a dynamical model, which reproduces the BOLD signal including the trend component, as described in Section II. Next, Section III presents the parameter optimization algorithm for the dynamical model and shows its prediction performance for data obtained by fMRI scanner in an experiment with visual stimuli. Finally, Section IV uses the traditional models, i.e., GLM, MRM, and BM, to predict BOLD signals from the same experimental data in order to compare them with our presented model.

II. DOUBLE OSCILLATION MODEL

This section introduces the model of the BOLD signals of voxels in the human visual cortex in response to the visual stimuli. The model is called “Double Oscillation Model”

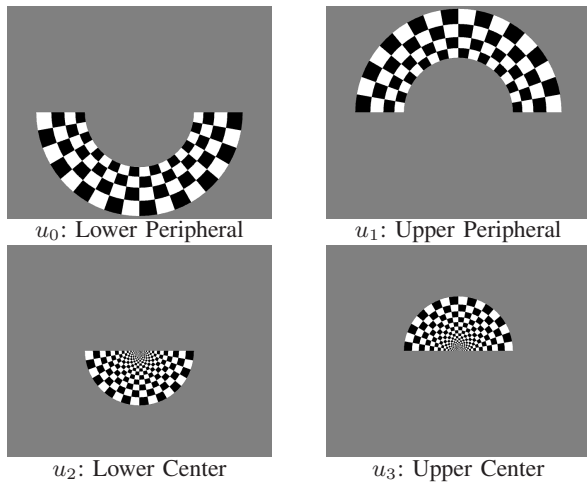


Fig. 2. Four types of visual stimuli.

(DOM) and described by the following equation:

$$\begin{aligned} \dot{v} &= -k_v v + \sum_j u_j w_j (v_{rj} - v), \\ \begin{pmatrix} \dot{p}_0 \\ \dot{p}_1 \end{pmatrix} &= \begin{pmatrix} k_{p0,0} & -k_{p0,1} \\ k_{p1,0} & -k_{p1,1} \end{pmatrix} \begin{pmatrix} p_0 \\ p_1 \end{pmatrix} + \begin{pmatrix} v \\ 0 \end{pmatrix}, \\ \begin{pmatrix} \dot{s}_0 \\ \dot{s}_1 \end{pmatrix} &= \begin{pmatrix} k_{s0,0} & -k_{s0,1} \\ k_{s1,0} & -k_{s1,1} \end{pmatrix} \begin{pmatrix} s_0 \\ s_1 \end{pmatrix} + \begin{pmatrix} k_s v \\ 0 \end{pmatrix}, \\ \hat{y} &= p_0 + s_0 + y_b \end{aligned}$$

where $v \in \mathbb{R}$, $\mathbf{p} = (p_0, p_1)^T \in \mathbb{R}^2$, and $\mathbf{s} = (s_0, s_1)^T \in \mathbb{R}^2$ are the internal states, $\hat{y} \in \mathbb{R}$ is the predicted BOLD signal, $u_j \in \{0, 1\}$ for $j = \{0, \dots, N_u - 1\}$ denote visual stimuli, the parameter N_u denotes the number of the visual stimuli, $u_j = 1$ denotes the presence of the stimulus u_j , and $u_j = 0$ denotes the absence. Each parameter $v_{rj} \in \mathbb{R}$ can be regarded as a reversal potential of v corresponding to the stimulus u_j , and the parameter $w_j \in \mathbb{R}_0^+$ corresponds to its weight, where the character \mathbb{R}_0^+ denotes the set of nonnegative numbers. The parameters v_{rj} , w_j , and $k_v \in \mathbb{R}_0^+$ determine the dynamics of v . The parameter $k_p \in \mathbb{R}$ is the connection weight between the components \mathbf{p} and \mathbf{s} . The parameter $y_b \in \mathbb{R}$ is the offset of the predicted BOLD signal \hat{y} . The parameters $k_{p0,0}$, $k_{p0,1}$, $k_{p1,0}$, $k_{p1,1}$, $k_{s0,0}$, $k_{s0,1}$, $k_{s1,0}$, and $k_{s1,1} \in \mathbb{R}_0^+$ determine the dynamics of the two oscillating components \mathbf{p} and \mathbf{s} . Since the real parts of the eigenvalues of the matrix $k_{sn,m}$ corresponding to the dynamics of the oscillating component \mathbf{s} are smaller than those of \mathbf{p} (see Table I), the oscillating component \mathbf{p} is the main fast component and \mathbf{s} is the slow trend component. In addition, the state v represents the underlying neuronal activity. The internal states v , p_0 , p_1 , s_0 , and s_1 are initialized at the time 1. Therefore, the parameters summarized in Table I characterize the entire dynamics of DOM.

III. BOLD SIGNAL

For scanning BOLD signals, we have prepared the four types of visual stimuli shown in Fig. 2. The checkerboard

TABLE I
PARAMETERS OF DOM

Parameter	Initial	Scaling (10^{-3})	Example \mathcal{A}	Example \mathcal{B}
w_0	1	1	3.92	
w_1	1	1	7.67	
w_2	1	1	0.02	
w_3	1	1	0.29	
v_{r0}	5	5	7.13	
v_{r1}	5	5	8.48	
v_{r2}	5	5	-13.59	
v_{r3}	5	5	-9.32	
k_v	5	1	1.83	
$k_{p0,0}$	0.5	1	-0.03	
$k_{p0,1}$	1	0	1.00	ditto
$k_{p1,0}$	1	1	0.20	
$k_{p1,1}$	1	1	1.42	
$k_{s0,0}$	0.05	0.1	0.013	
$k_{s0,1}$	0.1	0	0.100	
$k_{s1,0}$	0.1	0.1	0.013	
$k_{s1,1}$	0.1	0.1	0.033	
k_s	0.05	0.1	0.026	
y_b	0	1	491.8	
$v(1)$	0	0.01	0.00	-8.37
$p_0(1)$	0	1	-2.32	9.06
$p_1(1)$	0	1	6.88	9.96
$s_0(1)$	0	0.1	0.01	0.40
$s_1(1)$	0	0.1	0.01	5.00

images flickering at 10 Hz are called “Lower Peripheral”, “Upper Peripheral”, “Lower Center”, and “Upper Center”, labeled as u_0 , u_1 , u_2 , and u_3 , respectively. Recall that $u_j = 1$ denotes the presence of the visual stimulus u_j and $u_j = 0$ denotes its absence. We scanned whole brain T_2^* -weighted fMRI images by using a 3T fMRI scanner Magnetom Trio (Siemens AG [22]) with 30 ms echo time (TE = 30 ms) and 3 second repetition time (TR = 3 s). Each scan consists of 50 contiguous slices with 3 mm thickness; Each slice is an image of 64×64 pixels and $3 \text{ mm} \times 3 \text{ mm}$ in-plane resolution. Thus, 204,800 voxels are scanned in total. We selected region of interest (ROI) corresponding to which the detrended time series have a large correlation coefficient ($r > 0.20$) with any of the visual stimulus time series u_j , where “detrend” implies that the low frequency component ($f < 1/120$ Hz) is removed from the BOLD signal time series by using Fourier transformation, hereafter. The number of voxels in the ROI is 155.

The variable n denotes the n -th sample time; $u_j(n)$ denotes the value of the visual stimulus u_j and $y(n)$ denotes the scanned BOLD signal of a voxel at the n -th sample time. The number of scans N is 252. Since a slice is in the transverse plane (plane dividing a body into upper and lower parts), the scan timing of a voxel depends on the position of the voxel on the superior-inferior axis. In other words, the n -th scanned BOLD signal $y(n)$ is delayed by τ_d compared to the n -th applied visual stimulus $u_j(n)$, where the delay time τ_d is called the *scan delay*, hereafter. The experiments are performed twice; They are labeled with the subscripts \mathcal{A} and \mathcal{B} implying that the subscripted variable corresponds to Experiment \mathcal{A} and \mathcal{B} , hereafter, e.g., the variable $y_{\mathcal{A}}$ denotes the scanned BOLD signal time series y for Experiment \mathcal{A} .

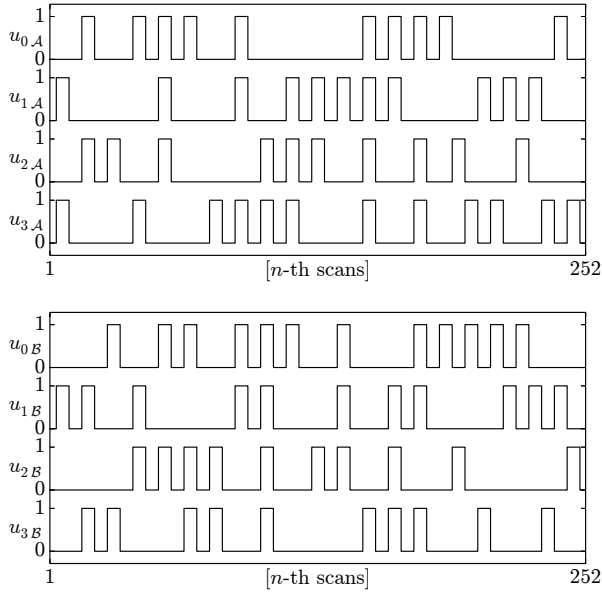


Fig. 3. Visual stimulus time series u_j . Each visual stimulus $u_j(n)$ has a binary state: present ($u_j = 1$) and absent ($u_j = 0$). (Top) u_{jA} of Experiment \mathcal{A} , (Bottom) u_{jB} of Experiment \mathcal{B} .

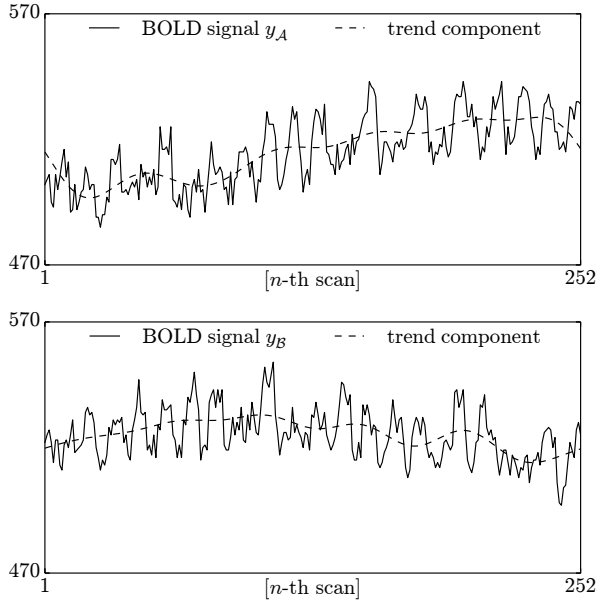


Fig. 4. The scanned BOLD signal time series y . (Top) y_A of Experiment \mathcal{A} , (Bottom) y_B of Experiment \mathcal{B} .

Fig. 3 shows the time series of the visual stimuli u_j . Fig. 4 shows an example scanned BOLD signal time series y of a voxel in the ROI.

Prediction Performance: The scanned BOLD signal time series y_A is used for parameter optimization and y_B is used for validation of the model, i.e., as a measure of generalization ability. The term $\hat{y}(n)$ denotes the BOLD signal predicted by a model corresponding to the scanned

BOLD signal y . The prediction performances are evaluated as the root mean square errors (RMSE) between the scanned BOLD signal time series y and the corresponding predicted BOLD signal time series \hat{y} :

$$\text{RMSE} = \frac{1}{N} \sqrt{\sum_{n=1}^N (y(n) - \hat{y}(n))^2}.$$

In addition, the prediction performance is also evaluated by the *Schwarz information criterion* (SIC) [23], which is as follows:

$$\text{SIC} = N \log \text{RMSE}^2 + k \log N,$$

where k denotes the *Degrees of Freedom* (DOF). The DOF k of DOM is generally $(11 - 2) + 5 + 2N_u = 22$ since DOM has 11 parameters, in which 2 parameters $k_{p_{0,1}}$ and $k_{s_{0,1}}$ are clamped to the default values, 5 internal states, and 2 parameters for each visual stimulus. Note that, the smaller the RMSE and the SIC are, the better the prediction performances are.

For parameter optimization, the detrended scanned BOLD signal time series y_A is calculated and is denoted by y_A^{det} , where the superscript det denotes that the superscripted variable corresponds to the detrended scanned BOLD signal time series y^{det} . The parameters are optimized by an algorithm consisting of three processes. The first process optimizes the parameters of DOM to predict the detrended scanned BOLD signal time series y_A^{det} , and the second and third processes try to predict the original scanned BOLD signal time series y_A by using a random search algorithm. We have confirmed that this three-step process leads to a better prediction performance than a simple one-step process.

Parameter Optimization Algorithm:

1) First Process.

- The parameter values summarized in the first column “Initial” in Table I are denoted by \mathbf{P}^{old} .
- y_b is initialized to be the minimal value of y_A^{det} .
- RMSE^{old} is set to a large enough value (10^8 in this paper).
- The following sub-process is repeated until it converges, where $\mathbf{P}^{\text{change}} = \{w_j, k_{p_{n,m}}, u_b, y_b, p_0(1), p_1(1)\}$, $y^{\text{teacher}} = y_A^{\text{det}}$, and the internal state $\mathbf{s} = (s_0, s_1)^T$ is clamped to $(0, 0)^T$.

Sub-process.

- The parameter values are set to \mathbf{P}^{old} .
- The parameter values only denoted in $\mathbf{P}^{\text{change}}$ are changed by the values which have a uniform distribution $\mathcal{U}(-a, a)$, where the parameter a corresponding to the parameters are summarized in the second column “Scaling” in Table I and are denoted by \mathbf{P}^{new} .
- The predicted BOLD signal time series \hat{y} is generated.
- The RMSE between y^{teacher} and \hat{y} is calculated and is denoted by RMSE^{new} .

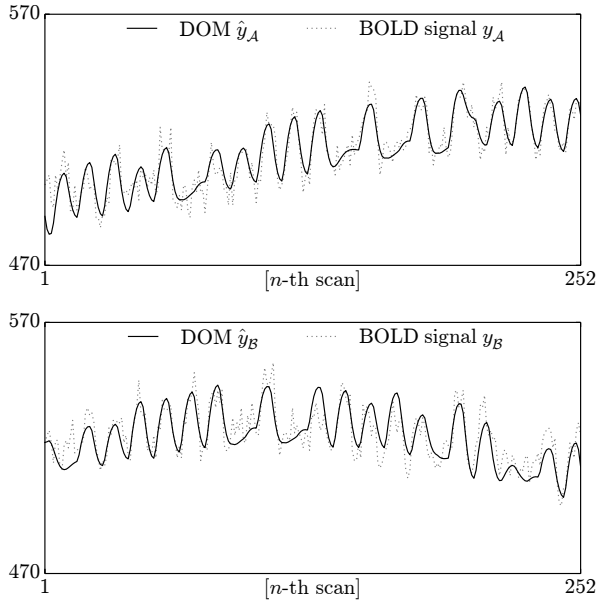


Fig. 5. The BOLD signal time series \hat{y} predicted by DOM. (Top) \hat{y}_A of Experiment \mathcal{A} with $\text{RMSE}_A = 5.54$, $\text{SIC} = 984$. All parameters are optimized, which are summarized in the third column “Example $_A$ ” of Table I. (Bottom) \hat{y}_B of Experiment \mathcal{B} with $\text{RMSE}_B = 6.28$. Only the initial internal states are optimized, which are also summarized in the fourth column “Example $_B$ ” of Table I, and the other parameters equal to those of the upper figure.

- If $\text{RMSE}^{\text{new}} < \text{RMSE}^{\text{old}}$, RMSE^{old} is updated to RMSE^{new} and \mathbf{P}^{old} is updated to \mathbf{P}^{new} .
- If RMSE^{old} is not updated many times (10^4 in this paper), this sub-process is considered to be converged and is finished. Otherwise, this sub-process is repeated.

2) Second process.

- Next, y_b is initialized to be the minimal value of y_A .
- RMSE^{old} is set to a large enough value.
- The above sub-process is repeated until it converges, where $\mathbf{P}^{\text{change}} = \{k_{sn,m}, p_b, s_b, y_b, s_0(1), s_1(1)\}$, and $y^{\text{teacher}} = y_A$.

3) Third process.

- Finally, the above sub-process is repeated until it converges, where $\mathbf{P}^{\text{change}}$ is the set of all the parameters of DOM and $y^{\text{teacher}} = y_A$.
- After convergence, the parameter values \mathbf{P}^{old} are used as the parameters and the initial values of the internal states of the DOM corresponding to the scanned BOLD signal time series y_A .

The BOLD signal time series \hat{y}_A predicted by DOM is shown in the upper figure of Fig. 5, which confirms that DOM has a good performance on prediction of the scanned BOLD signal time series y_A . The prediction performance is evaluated as $\text{RMSE}_A = 5.54$ and $\text{SIC} = 984$. y_B is measured by the following algorithm for generalization ability comparison;

Model Validation Algorithm:

- The parameter values are set to \mathbf{P}^{old} in the third process.
- RMSE^{old} is set to a large enough value.
- The above sub-process is repeated until it converges, where $\mathbf{P}^{\text{change}} = \{p_0(1), p_1(1), s_0(1), s_1(1)\}$, $y^{\text{teacher}} = y_B$.
- After convergence, the parameter values $p_0(1)$, $p_1(1)$, $s_0(1)$, and $s_1(1)$ in \mathbf{P}^{old} are used as the initial internal states of the DOM corresponding to the scanned BOLD signal time series y_B .

Note that the scanned BOLD signal time series y_B is used only for the initial internal state estimation for the time series but not for parameter optimization. Recall that lower RMSE_B implies a better generalization ability, i.e., a more valid model. The BOLD signal time series \hat{y}_B predicted by DOM is also shown in the lower figure of Fig. 5. The prediction performance is evaluated as $\text{RMSE}_B = 6.28$; Since RMSE_B is only little more than RMSE_A , DOM has a good generalization ability.

IV. EXISTING MODELS FOR COMPARISON

This section introduces the existing models for comparison.

General Linear Model: The General Linear Model (GLM) [4]–[9] predicts the BOLD signal time series $y(n)$ to be a summation of convolutions between the visual stimuli $u_j(n)$ and the hemodynamic response function $\text{HRF}(m)$:

$$\hat{y}(n) = \sum_j w_j \sum_{m \geq 0} \text{HRF}_j(m) u_j(n - m) + c,$$

where w_j is an input weight corresponding to the visual stimulus u_j . The hemodynamic response function HRF_j corresponding to the visual stimulus u_j is a finite impulse response (FIR) filter with the length d and c denotes the constant bias. This paper estimates HRF_j by using the method presented in [24], where the original method clamps $\text{HRF}_j(0)$ to 0, but this paper clamps $\text{HRF}_j(-1)$ to 0 because of the scan delay τ_d . The filter length d is set to $d = 10$ corresponding to 30 s, which is sufficiently long [24], [25]. The hyperparameters, the smoothness factor h , the strength of the prior ν , and the noise level σ , are initialized to $1/9$, 1, and 10^2 , and optimized to maximize the likelihood function $p(\hat{y}_A | u_j, \sigma, \nu, h)$. Since GLM has no internal states, the prediction of the BOLD signal time series y_B for validation is calculated straightforwardly. The DOF k of GLM is $d \times N_u + 1 = 41$ in the experiments.

The BOLD signal time series \hat{y}_A and \hat{y}_B predicted by GLM are shown Fig. 6 and the prediction performance is evaluated as $\text{RMSE}_A = 10.62$, $\text{SIC} = 1418$, and $\text{RMSE}_B = 13.92$. Although the scanned BOLD signal time series y_A increases gradually, the BOLD signal time series \hat{y}_A predicted by GLM cannot reproduce such a feature. In other words, GLM cannot predict the trend component. The error increases in the case of the scanned BOLD signal time series y_B for validation.

Recall that the BOLD signal is often detrended [6], [19]–[21]. Since detrending is performed by Fourier transformation, the trend component ($f < 1/120$ Hz) is reconstructed

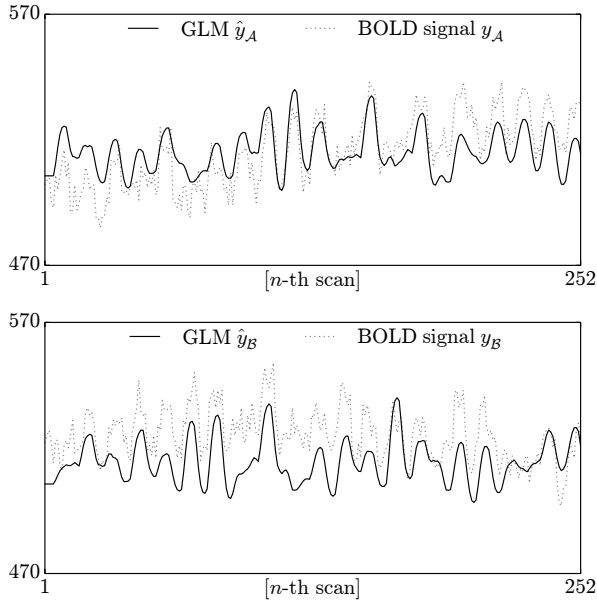


Fig. 6. The BOLD signal time series \hat{y} predicted by GLM. (Top) \hat{y}_A of Experiment \mathcal{A} predicted by GLM with $\text{RMSE}_A = 10.62$ and $\text{SIC} = 1418$, (Bottom) \hat{y}_B of Experiment \mathcal{B} with $\text{RMSE}_B = 13.92$.

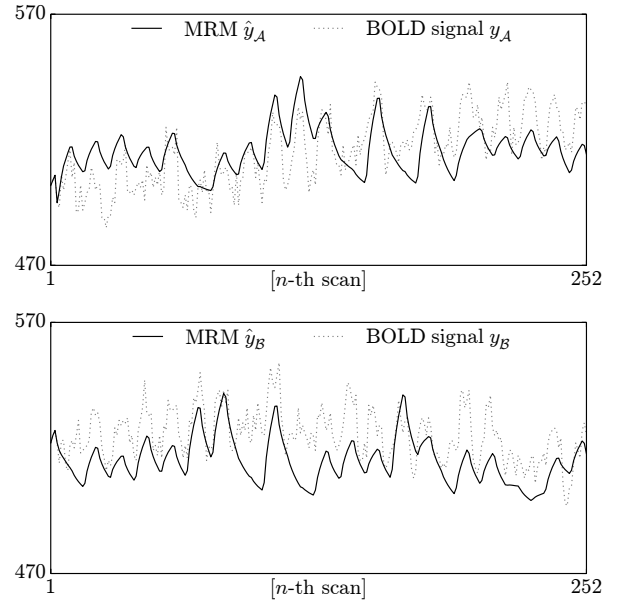


Fig. 8. The BOLD signal time series \hat{y} predicted by MRM. (Top) \hat{y}_A of Experiment \mathcal{A} with $\text{RMSE}_A = 9.69$ and $\text{SIC} = 1261$, (Bottom) \hat{y}_B of Experiment \mathcal{B} with $\text{RMSE}_B = 11.45$.

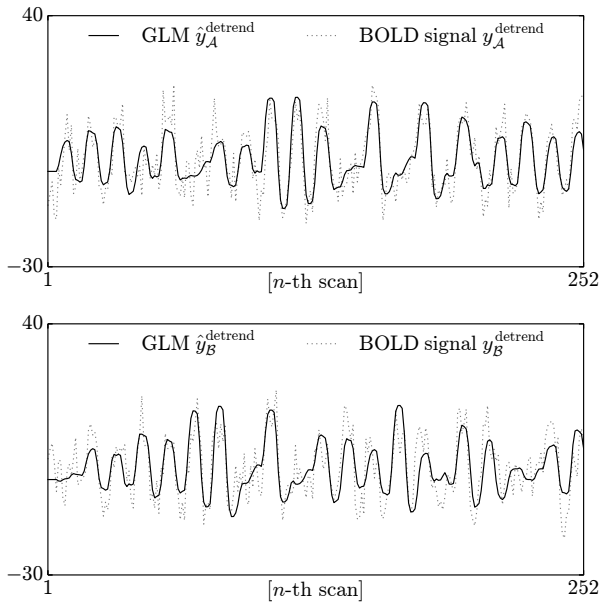


Fig. 7. The detrended BOLD signal time series \hat{y}^{det} predicted by GLM. (Top) \hat{y}_A^{det} of Experiment \mathcal{A} with $\text{RMSE}_A^{\text{det}} = 5.17$ and $\text{SIC}^{\text{det}} = 1121$, (Bottom) \hat{y}_B^{det} of Experiment \mathcal{B} with $\text{RMSE}_B^{\text{det}} = 5.73$.

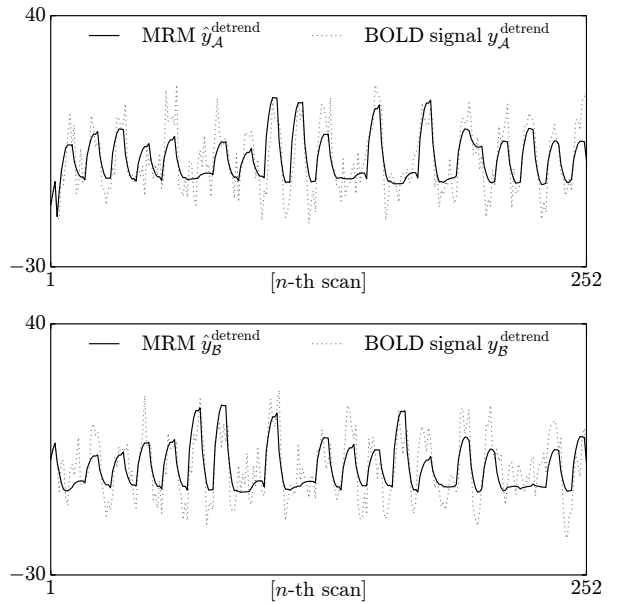


Fig. 9. The detrended BOLD signal time series \hat{y}^{det} predicted by MRM. (Top) \hat{y}_A^{det} of Experiment \mathcal{A} with $\text{RMSE}_A^{\text{det}} = 5.54$ and $\text{SIC}^{\text{det}} = 1045$, (Bottom) \hat{y}_B^{det} of Experiment \mathcal{B} with $\text{RMSE}_B^{\text{det}} = 5.80$.

by inverse Fourier transformation. The reconstruction requires 13 parameters (or initial internal states) since the trend components ($f < 1/120$ Hz) are scored in 13 bins when the number of scans $N = 252$ and the repetition time $\text{TR} = 3$ s. The reconstructed trend components corresponding to y_A and y_B are denoted by y_A^{trend} and y_B^{trend} , which are shown in Fig. 4 with the dashed lines. Since both Fourier transformation and GLM have a constant bias, the DOF k^{det} of GLM in the case of detrending is $k^{\text{det}} = k + 13 - 1 = 52$. GLM also predicts the

detrended BOLD signal time series \hat{y}_A^{det} and \hat{y}_B^{det} , which are shown in Fig. 7, and the prediction performance is evaluated as $\text{RMSE}_A^{\text{det}} = 5.17$, $\text{SIC}^{\text{det}} = 1121$, and $\text{RMSE}_B^{\text{det}} = 5.73$. In the case of detrending, RMSEs of GLM are not as bad as in the case without detrending. However, the SIC still remains large.

Multivariable Regressive Model: The Multivariable Regressive Model (MRM) estimates the BOLD signal $y(n)$ to be predicted by the past values $\hat{y}(n - m)$ and $u_j(n - m)$ of

the same time series y and the visual stimuli u_j :

$$\hat{y}(n) = \sum_j \sum_{p>m\geq 0} k_j(m)u_j(n-m) + \sum_{q\geq m\geq 1} l(m)\hat{y}(n-m) + y_b,$$

where p and q are the orders of this model, and $k_j(m)$ and $l(m)$ are parameters with the lengths p and q . Because of the scan delay τ_d , the visual stimuli $u_j(n)$ are past values of the predicted BOLD signal $\hat{y}(n)$. Thus, this paper employs $p = 2$. Note that this is a special case of the Granger Causality Analysis (GCA) [10]–[13], where GCA additionally takes into account the effects of other voxels.

The parameters $k_j(m)$ and $l(m)$ are optimized by using the least squares method under the assumption that the predicted sequence of past values $\hat{y}(n-m)$ equals that of the scanned past values $y(n-m)$; This assumption can be regarded as an internal state estimation since the predicted past values \hat{y} are the internal states from a dynamical system viewpoint [26]. The initial internal states (i.e., $\hat{y}(k)$, $-q \leq k \leq -1$) are estimated by using the EM algorithm [27] with consideration of the whole scanned BOLD signal time series $y(n)$, $n = 1, 2, \dots, N$. The DOF k of MRM is $2q + pN_u + 1$, where MRM has q parameters of $l(m)$, the bias term y_b , q internal states, and p parameters of $k_j(m)$ for each visual stimulus.

We examined several values of q and found that $q = 6$ shows the best prediction performance in RMSE and SIC. Thus, the DOF k of MRM is 21 in the experiments. The BOLD signal time series \hat{y}_A and \hat{y}_B predicted by MRM are shown in Fig. 8 and the prediction performance is $\text{RMSE}_A = 9.69$, $\text{SIC} = 1261$, and $\text{RMSE}_B = 11.45$. Although, in contrast to GLM, MRM can partially reproduce the gradually increasing trend component of the given BOLD signal time series y_A , it has little generalization ability; it cannot reproduce the trend component in the BOLD signal time series y_B . In addition, it lacks the rapid change of the BOLD signal. As a result, the prediction performance of MRM is as bad as that of GLM. In the case of detrending shown in Fig. 9, MRM can reproduce the scanned BOLD signal time series y_A^{det} with the prediction performance: $\text{RMSE}_A^{\text{det}} = 5.54$, $\text{SIC}^{\text{det}} = 1045$, and $\text{RMSE}_B^{\text{det}} = 5.80$. As in the case of GLM, the SIC is still large.

Balloon Model: The Balloon Model is a four-dimensional nonlinear dynamical model of the hemodynamic response [14]–[17]. It takes account of the changes of the cerebral blood flow (CBF), the cerebral metabolic rate of oxygen (CMRO₂) and the cerebral blood volume (CBV) accompanying the CBF. The equations describing the dynamics of BM [15] are omitted due to the page length limitation. This paper employs the BM implemented in SPM [15], [25] for Bayesian parameter optimization [28] and time series prediction, where the implemented BM is a component of Dynamic Causal Modelling (DCM) [28]–[30]; DCM is a model of interactions among neuronal populations and employs the BM as the model of the BOLD signals in response to the neuronal populations. Since this paper focuses on the BOLD signal of a single voxel, the number of regions is 1 and no

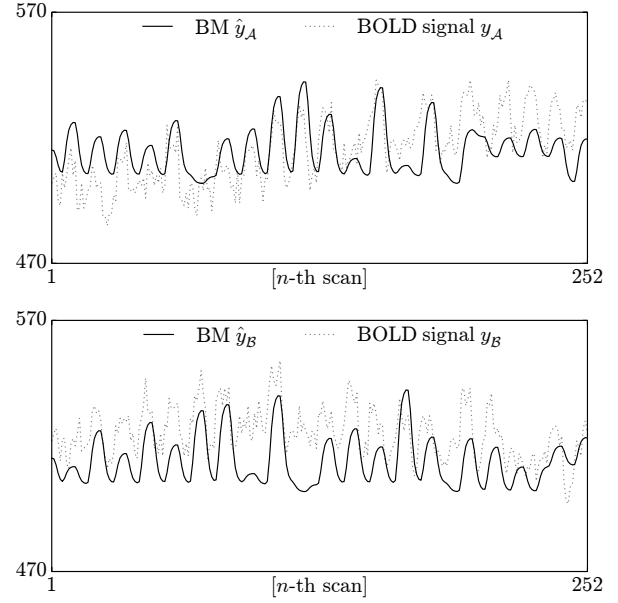


Fig. 10. The BOLD signal time series \hat{y} predicted by BM. (Top) \hat{y}_A of Experiment \mathcal{A} with $\text{RMSE}_A = 11.27$ and $\text{SIC} = 1280$, (Bottom) \hat{y}_B of Experiment \mathcal{B} with $\text{RMSE}_B = 13.60$.

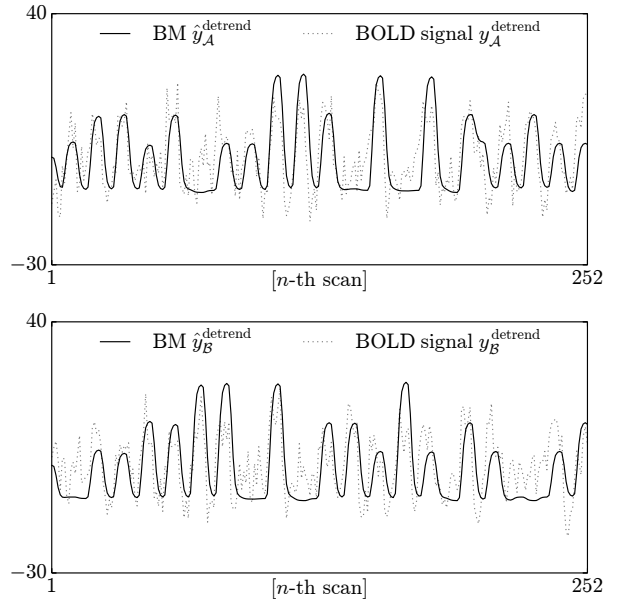


Fig. 11. The detrended BOLD signal time series \hat{y}^{det} predicted by BM. (Top) \hat{y}_A^{det} of Experiment \mathcal{A} with $\text{RMSE}_A^{\text{det}} = 5.94$ and $\text{SIC}^{\text{det}} = 1025$, (Bottom) \hat{y}_B^{det} of Experiment \mathcal{B} with $\text{RMSE}_B^{\text{det}} = 6.05$.

interactions are assumed. BM implemented in SPM can also take the scan delay τ_d into account. The DOF k of BM is $5 + 2 + 2 + N_u = 13$, where the BM has 5 parameters, and DCM has 2 parameters determining the dynamics of the neuronal populations, the intercept term, the scale term, and 1 parameter for each visual stimulus. Note that although BM has 4 internal states and DCM has 1 internal state corresponding to the neuronal population, SPM estimates only the parameters by using the EM algorithm but does

TABLE II
AVERAGE OF NORMALIZED RMSE

Model	without detrending		with detrending	
	NRMSE _A	NRMSE _B	NRMSE _A ^{det}	NRMSE _B ^{det}
DOM	0.78	1.07	(0.78)	(1.07)
GLM	1.00	1.69	0.72	0.82
MRM	1.01	1.64	0.74	0.82
BM	1.06	1.70	0.80	0.88

The average of the RMSE between the scanned BOLD signal time series y and the BOLD signal time series \hat{y} predicted by each model, where the RMSE of GLM in each voxel is normalized to 1 and is called NRMSE. NRMSE_A denotes the NRMSE for Experiment \mathcal{A} , whose time series $y_{\mathcal{A}}$ is used for parameter optimization. NRMSE_B denotes the NRMSE for Experiment \mathcal{B} , whose time series $y_{\mathcal{B}}$ is used for validation of the model, i.e., for measuring the generalization ability. The superscript ^{det} implies that the scanned BOLD signal time series y is detrended by using Fourier transformation.

TABLE III
AVERAGE OF SIC

Model	without detrending		with detrending	
	DOF k	SIC	DOF k^{det}	SIC ^{det}
DOM	22	1064	(22)	(1064)
GLM	41	1307	53	1194
MRM	21	1199	33	1095
BM	13	1180	25	1091

The average of the SIC [23] for Experiment \mathcal{A} . In the case of detrending, the DOF is increased by 12, since it requires the reconstruction of the trend components ($f < 1/120$ Hz), which are scored in 13 bins and the constant bias is duplicated.

not estimate the initial internal states, which are clamped to 0.

In both the cases concerning with and without detrending, BM shows the worst prediction performance as shown Figs. 10 and 11.

Comparison: The prediction performances of DOM and the existing models are evaluated as the RMSE and the SIC. For fair comparison, RMSE_A of GLM is normalized to 1 for each voxel and called the normalized RMSE (NRMSE). Table II summarizes the average of the NRMSE for all the 155 voxels in the ROI. DOM shows the smallest NRMSE_A and NRMSE_B, which implies that DOM is the best way to predict BOLD signal time series in the case without detrending. Furthermore, NRMSE_A and NRMSE_B for DOM are not so much larger than NRMSE_A^{det} and NRMSE_B^{det} for the other models; DOM provides an alternative way to detrend.

Even if detrending by using Fourier transformation improves the RMSEs, the reconstruction of the trend component by using inverse Fourier transformation requires additional parameters; Detrending impairs the SIC. Thus, DOM shows the best SIC, where Table III summarizes the average of the SIC. Note that, since the SIC value contains the logarithm of the RMSE, multiple SIC values are compared by the difference, but not by the proportion.

V. CONCLUSION

This paper presented a nonlinear dynamical model called *Double Oscillation Model* (DOM) to predict the BOLD signal time series. In comparison with the traditional models,

i.e., General Linear Model, Multivariable Regressive Model, and Balloon Model, the DOM has the best prediction performance in the absence of detrending. DOM does not require detrending, which could destroy and ignore the dynamics and relationships of voxels. Thus, DOM helps in finding the dynamics of voxels and correlation between voxels which have been ignored as trend component by existing models.

The authors would like to thank Professor Toshimitsu Ushio of Osaka University for helpful discussions. This work was partially supported by Grant-in-Aid for JSPS Fellows.

REFERENCES

- [1] W. Chen *et al.*, "Mapping of lateral geniculate nucleus activation during visual stimulation in human brain using fMRI." *Magnetic Resonance in Medicine*, vol. 39, no. 1, pp. 89–96, 1998.
- [2] K. A. Schneider *et al.*, "Retinotopic organization and functional subdivisions of the human lateral geniculate nucleus: a high-resolution functional magnetic resonance imaging study." *The Journal of Neuroscience*, vol. 24, no. 41, pp. 8975–85, 2004.
- [3] K. A. Schneider and S. Kastner, "Visual responses of the human superior colliculus: a high-resolution functional magnetic resonance imaging study." *Journal of Neurophysiology*, vol. 94, no. 4, pp. 2491–503, 2005.
- [4] K. J. Friston and A. Holmes, "Statistical parametric maps in functional imaging: a general linear approach." *Human brain Mapping*, vol. 2, no. 4, pp. 189–210, 1994.
- [5] K. J. Friston *et al.*, "Analysis of fMRI time-series revisited." *NeuroImage*, vol. 2, no. 1, pp. 45–53, 1995.
- [6] F. G. Meyer, "Wavelet-based estimation of a semiparametric generalized linear model of fMRI time-series." *IEEE Transactions on Medical Imaging*, vol. 22, no. 3, pp. 315–22, 2003.
- [7] D. Bressler *et al.*, "Negative BOLD fMRI response in the visual cortex carries precise stimulus-specific information." *PLoS ONE*, vol. 2, no. 5, p. e410, 2007.
- [8] R. Leech and D. Leech, "Testing for spatial heterogeneity in functional MRI using the multivariate general linear model." *IEEE Transactions on Medical Imaging*, vol. 30, no. 6, pp. 1293–302, 2011.
- [9] K. Lee *et al.*, "A data-driven sparse GLM for fMRI analysis using sparse dictionary learning with MDL criterion." *IEEE Transactions on Medical Imaging*, vol. 30, no. 5, pp. 1076–89, 2011.
- [10] R. Goebel *et al.*, "Investigating directed cortical interactions in time-resolved fMRI data using vector autoregressive modeling and Granger causality mapping." *Magnetic Resonance Imaging*, vol. 21, no. 10, pp. 1251–1261, 2003.
- [11] A. Roebroeck *et al.*, "Mapping directed influence over the brain using Granger causality and fMRI." *NeuroImage*, vol. 25, no. 1, pp. 230–42, 2005.
- [12] D. Marinazzo *et al.*, "Nonlinear connectivity by Granger causality." *NeuroImage*, vol. 58, no. 2, pp. 330–8, 2011.
- [13] W. Tang *et al.*, "Measuring Granger causality between cortical regions from voxelwise fMRI BOLD signals with LASSO." *PLoS Computational Biology*, vol. 8, no. 5, p. e1002513, 2012.
- [14] R. B. Buxton and L. R. Frank, "A model for the coupling between cerebral blood flow and oxygen metabolism during neural stimulation." *Journal of Cerebral Blood Flow & Metabolism*, vol. 17, no. 1, pp. 64–72, 1997.
- [15] R. B. Buxton *et al.*, "Dynamics of blood flow and oxygenation changes during brain activation: the balloon model." *Magnetic Resonance in Medicine*, vol. 39, no. 6, pp. 855–64, 1998.
- [16] —, "Modeling the hemodynamic response to brain activation." *NeuroImage*, vol. 23 Suppl 1, pp. S220–33, 2004.
- [17] S. M. Smith *et al.*, "Network modelling methods for FMRI." *NeuroImage*, vol. 54, no. 2, pp. 875–91, 2011.
- [18] P. A. Bandettini *et al.*, "Processing strategies for time-course data sets in functional MRI of the human brain." *Magnetic Resonance in Medicine*, vol. 30, no. 2, pp. 161–73, 1993.
- [19] R. D. Nowak, "Wavelet-based Rician noise removal for magnetic resonance imaging." *IEEE Transactions on Medical Imaging*, vol. 8, no. 10, pp. 1408–19, 1999.

- [20] K. L. Miller *et al.*, "Nonlinear temporal dynamics of the cerebral blood flow response," *Human Brain Mapping*, vol. 13, no. 1, pp. 1–12, 2001.
- [21] J. Tanabe *et al.*, "Comparison of detrending methods for optimal fMRI preprocessing," *NeuroImage*, vol. 15, no. 4, pp. 902–7, 2002.
- [22] "Siemens." url: <http://www.siemens.com/entry/cc/en/>
- [23] G. Schwarz, "Estimating the Dimension of a Model," *The Annals of Statistics*, vol. 6, no. 2, pp. 461–464, 1978.
- [24] C. Goutte *et al.*, "Modeling the haemodynamic response in fMRI using smooth FIR filters." *IEEE Transactions on Medical Imaging*, vol. 19, no. 12, pp. 1188–201, 2000.
- [25] "SPM - Statistical Parametric Mapping." url: <http://www.fil.ion.ucl.ac.uk/spm/>
- [26] H. Kantz and T. Schreiber, *Nonlinear Time Series Analysis*. Cambridge University Press, 2004.
- [27] Z. Ghahramani and G. E. Hinton, "Parameter Estimation for Linear Dynamical Systems," *University of Toronto technical report CRGTR962*, vol. 6, no. CRG-TR-96-2, pp. 1–6, 1996.
- [28] K. J. Friston, "Bayesian estimation of dynamical systems: an application to fMRI." *NeuroImage*, vol. 16, no. 2, pp. 513–30, 2002.
- [29] K. J. Friston *et al.*, "Dynamic causal modelling," *NeuroImage*, vol. 19, no. 4, pp. 1273–1302, 2003.
- [30] K. E. Stephan *et al.*, "Nonlinear dynamic causal models for fMRI." *NeuroImage*, vol. 42, no. 2, pp. 649–62, 2008.